Thermal conductivity of the nematic liquid crystal 4-*n*-pentyl-4′-cyanobiphenyl

Guenter Ahlers, David S. Cannell, Lars Inge Berge,* and Shinichi Sakurai†
Department of Physics and Center for Nonlinear Science, University of California, Santa Barbara, California 93106
(Received 26 July 1993)

We report experimental results for the thermal conductivities of 4-*n*-pentyl-4′-cyanobiphenyl (5CB) for 19 °C < *T* < 48 °C. For $T < T_{NI} = 35.17$ °C this substance is a nematic liquid crystal, where T_{NI} is the nematic-isotropic transition temperature. The conductivities were determined by measuring the temperature difference across a horizontal layer of the fluid heated from below in magnetic fields either parallel or perpendicular to the heat current. The field magnitude was much larger than the Fréedericksz field. For $T < T_{NI}$, this yielded monodomain samples with the director oriented parallel to the field, and thus the conductivities $\lambda_\parallel$ and $\lambda_\perp$ with the director parallel and perpendicular to the heat current, respectively.

PACS number(s): 61.30.Eb, 66.60.+a, 44.90.+c, 64.70.Ja

I. INTRODUCTION

Although equilibrium properties of nematic liquid crystals have been studied extensively, there has been considerably less quantitative work on transport properties. These properties are of interest in themselves, and one would like to understand, for instance, the temperature dependence of the thermal conductivities from the viewpoint of a theory of the nematic state [1]. We hope that our measurements will make a contribution from this point of view. However, the immediate motivation for our investigation was rather different. In recent years, it has been recognized that convection in a nematic liquid crystal heated from below provides an interesting, rich system for the study of pattern formation under nonequilibrium conditions. After a number of early qualitative investigations [2–7], quantitative theoretical predictions [8] and experimental measurements [9] have become available only very recently. It turns out that the predictions are heavily dependent upon a knowledge of the thermal conductivity of the fluid. For a nematic liquid crystal, this conductivity is anisotropic, with values $\lambda_\parallel$ and $\lambda_\perp$ parallel and perpendicular to the director, respectively. So far as we know, there are no direct measurements of either $\lambda_\parallel$ or $\lambda_\perp$ for the nematic liquid crystal 4-*n*-pentyl-4′-cyanobiphenyl (5CB), which was used in the convection experiments. The only information available heretofore is based on unpublished indirect determinations [10] of the corresponding thermal diffusivities at a single temperature (25 °C) from forced Rayleigh light scattering [11], and these measurements have an accuracy of 10% or so. In the present paper we report direct measurements of $\lambda_\parallel$ and $\lambda_\perp$ which have an accuracy of 1% or 2% and a precision of 0.1%. They determine the ratio $\lambda_\parallel/\lambda_\perp$ with an accuracy of 0.5% over the entire nematic temperature range, and permit a much more stringent comparison between predictions and experiments for the bifurcation to Rayleigh-Bénard convection in this system. This comparison was carried out in another paper [9]. Here we report in detail on our measurements of the conductivities.

II. EXPERIMENTAL METHOD AND APPARATUS

A. Methods

The most direct method for the determination of the conductivity consists of a measurement of the temperature difference ΔT across a thin layer of the fluid in the presence of a heat current perpendicular to this layer. In the absence of convection and for sufficiently small ΔT, this gives

$$\lambda = Qd/A\Delta T , \tag{1}$$

where Q is the total heat current, d the layer thickness, and A the area of the sample perpendicular to the current. As will be discussed in detail in the next section, in practice it is necessary to make corrections for the conductance of sidewalls or other parallel paths for heat conduction, and for any series resistance due to the plates which confine the sample. For the study of a nematic liquid crystal, this method was used for instance by Pieranski and co-workers [12,13], who made measurements for *p*-methoxy benzylidene-*p*-*n*-butylaniline (MBBA). However, most work on liquid crystals has involved other, less direct methods. One of them is based on forced Rayleigh light scattering [10,11], and for a sample large compared to the scattering volume it yields the thermal diffusivity. Additional information about the density and heat capacity is then required to get the conductivity. Another method employs an acoustic technique [14]. In the present work, we have used the direct method of determining the temperature difference across a thin horizontal fluid layer in the presence of a heat current.

When heating a fluid layer in the presence of the gravitational field, an immediate concern is that the tempera-

*Present address: Department of Physics, University of Oslo, P.O. Box 1048 Blindern, 0316 Oslo, Norway.
†Permanent address: Department of Polymer Science and Engineering, Kyoto Institute of Technology, Matsugasaki, Sakyo-ku, Kyoto 606, Japan.

ture gradient might induce convection, which would enhance the heat transport. It turns out that convection can be avoided completely if the sample is horizontal (and thus the heat current and temperature gradient vertical). When heating from above, the fluid is then stably stratified, a lower portion being more dense than an upper one. In this case no convection will occur, provided the container geometry and thermal properties are chosen so as to avoid any unintended horizontal thermal gradients. It is perhaps less widely understood that a horizontal layer may also be heated from below without inducing flow, provided ΔT does not exceed the critical value ΔT_c for the onset of Rayleigh-Bénard (RB) convection [8,15]. In the present work we heated from below, because, in addition to the conductivity measurement, we also wanted to study the RB instability [9]. The value of ΔT_c depends on several fluid properties, on the magnetic field, and on the layer thickness [8]. We used two cells, designated as cell 2 and cell 3, of thickness 0.404 and 0.327 cm, respectively. For large horizontal fields, values of ΔT_c for cells 2 and 3 were approximately 5.2 and 11 °C, respectively, when the mean temperature was about 26 °C. For $\Delta T < \Delta T_c$, the measured conductivity was independent of ΔT. We show this in Fig. 1, which gives $\lambda_\perp$ as measured in cell 3 and in the presence of a large horizontal field. The measurements were made with the top of the sample held at 20.00 °C while varying the heat current. The bottom abscissa shows the mean temperature of the sample, and the top scale gives the temperature difference across the sample. The solid line is a fit to measurements made at various temperatures with temperature differences 2 °C or less. Clearly the measurements are essentially independent of ΔT until ΔT exceeds ΔT_c for Rayleigh-Bénard convection. When convection begins, the effective conductivity increases abruptly. The conductivity measurements reported in this paper were generally made with ΔT near 2 °C, and the measured value was assigned to the mean temperature. Very near T_{NI}, the nematic-isotropic transition

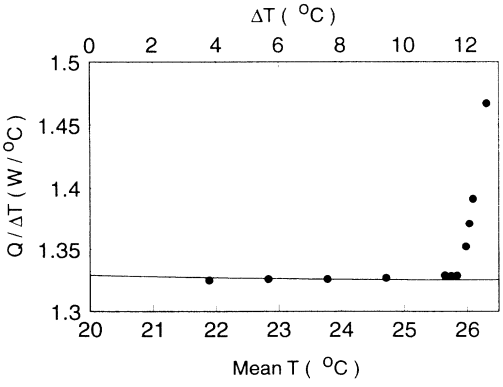

FIG. 1. Conductance of cell 3 when filled with 5CB. A horizontal field of 1000 G was applied. The top of the sample was at 20 °C. The bottom abscissa gives the mean temperature of the sample, and the top scale gives the temperature difference. For $\Delta T < 11.8$ °C, there is no evidence for a hydrodynamic contribution to the heat transport.

temperature, where particularly $\lambda_\parallel$ varies rapidly with T, even smaller values of ΔT were used, so that the assignment of the measured point to the mean temperature remained valid within our precision.

B. Apparatus

The apparatus was built primarily for the study of Rayleigh-Bénard convection in a thin horizontal layer of fluid heated from below [9]. At moderate heat currents, where the temperature difference ΔT across the fluid remained small, it was suitable for conductivity measurements. Our apparatus was an improved version of one described by Meyer, Ahlers, and Cannell [16], and is similar to others in use in our laboratory for the study of convection in isotropic fluids. A schematic diagram (not to scale [17]) is given in Fig. 2. It had a circular cross section. The base was made of poly(vinyl chloride) (PVC) [18]. The bath water entered and left through it, as indicated by the dashed lines with arrow heads, which indicate the flow direction. The flow rate was approximately 200 cm^3/s. Before entering the base, the bath water was cooled via a heat exchanger by a separate water circuit which was regulated by a Neslab Model RTE-110D refrigerated circulator and had a temperature stability of about 0.1 °C. The conductivity cell and its container (to be called the can) were located at the center of the apparatus. All electrical connections (not shown) were brought through a 0.63-cm-o.d. Tygon tube from the can through the bath to the base, where they were terminated at connectors. The incoming water passed over the bath thermistor [19], which in conjunction with an 8-Ω heater in the inlet section (not shown) was used to control the temperature [16,20]. The incoming temperature-controlled water flowed around the can and provided a stable thermal environment. The water then passed

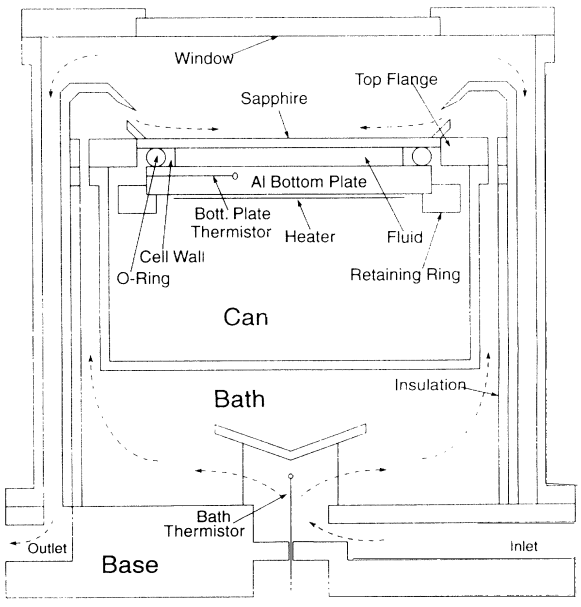

FIG. 2. Schematic diagram (not to scale, see Ref. [17]).

through a flow distributor, which directed it in the form of 30 jets over the top sapphire plate of the conductivity cell. There were three sets of jets, directed at three different radial locations. They were intended to provide uniform cooling of the top plate [16]. After passing over the sapphire top of the sample cell, the water returned outside of the incoming flow. It was collected in an annular channel (not shown) connected to the inlet side of a small centrifugal pump. Since its temperature had been raised by the heat flux through the cell by at most a few mK, it provided excellent thermal protection from any heat flux emanating from the outside through the sidewalls of the apparatus. A thin layer of insulating material (see Fig. 2) was provided between the incoming and outgoing water.

The top of the apparatus was a flange which contained an optically flat window with a diameter of 10 cm. Thus the sample could be viewed from above by a video camera. The main distinction of this apparatus relative to others in our laboratory is that it is constructed entirely of nonmagnetic materials so as to facilitate work in externally applied magnetic fields. The primary material of construction was aluminum. In order to make it corrosion resistant, all parts in contact with water were magnaplated [21]. All radial dimensions were kept reasonably small so that the apparatus would fit between the pole pieces of our magnet.

The cell was located in the can, which had an inner diameter of 12.76 cm and a height of 6.35 cm. The top plate of the cell was a single-crystal sapphire disk with a diameter of 10.16 cm and a thickness of 0.327 cm, which was sealed into the top flange of the can by an O-ring (not shown). The C axis was oriented perpendicular to the disk. The flatness of the disk was determined with an optical flat, and was found to be about 1 μm (four fringes) across the radius. The bottom plate was an aluminum disk with a diameter of 10.16 cm and a thickness of 1.11 cm. Its upper surface initially was diamond machined, but at later stages was polished. It was also flat to about 1 μm. We made no attempt to influence the director alignment by surface treatment. Rather, we depended upon using a large magnetic field to produce samples with either parallel or homeotropic alignment as desired. The cell wall was machined from Delrin, and had a height that was uniform to 5 μm. The seal which confined the fluid was provided by a Viton O-ring outside the Delrin cell wall, as shown in Fig. 2. The aluminum bottom plate was held up by an acryllic retaining ring, which in turn was attached by six No. 8-32 machine screws (not shown) to the top flange of the can. Adjusting the tension in the screws while examining the cell under an expanded laser beam made it possible to reduce the variation in the cell thickness to less than 2 μm.

A 90-Ω metal-film heater [22] with a diameter of 8.9 cm was attached with adhesive to the lower surface of the bottom plate of the cell to provide uniform heating. The temperature of the bottom plate was measured with a thermistor [19], which was epoxied into a hole that was 0.2 cm in diameter, 3.5 cm deep, and drilled radially inward from the side at the mid-height of the plate. The first 5 cm of the thermistor leads were placed in good thermal contact with the plate.

In our convection studies, we used three cell geometries, identified as cell 1, cell 2, and cell 3. Two of these (cell 2 and cell 3) were used also for the conductivity measurements to be reported here. For both of them, the sidewall had an annular horizontal cross section, with an inner diameter of 8.38 cm and an outer diameter of approximately 9.2 cm. The thickness was 0.404 ± 0.001 cm for cell 2 and 0.327 ± 0.001 cm for cell 3. The exterior side of the wall was shaped to the curvature of the Viton O-ring, which sealed the cell. Approximate centering of the sidewall underneath the sapphire was assured by an acryllic alignment ring (not shown in Fig. 2). Two fill lines [23] of 0.10 cm outer diameter passed through the O-ring and sidewall on opposite sides and were cut off flush with the inside of the wall. After the cell was filled, the two lines were connected [23] to each other and stored immediately below the cell bottom in the can. The cell bottom was protected thermally by three layers of "bubble" paper (not shown), with a combined thickness of about 0.6 cm, which was just adequate to fill the interior of the retaining ring. The space below the bubble paper and retaining ring contained only air. A layer of open-pore foam (not shown) surrounded the retaining ring and bottom plate and just filled the space between this ring, the plate, and the can wall.

The horizontal magnetic field for the measurement of $\lambda_\perp$ was provided by a 12-in. low-impedance Varian electromagnet (V-3600 Series) with a pole gap of about 19.5 cm. The pole pieces were shaped so as to optimize the uniformity of the field over the sample volume. We measured the field variation in the region of the sample, and found it to be no more than $\pm0.15\%$. Using a HP Model 6269B power supply, we were able to generate fields up to 1500 G. A characteristic Fréedericksz field is given by

$$H_f=(\pi/d)(k_{11}/\chi_a\rho)^{1/2}\ . \tag{2}$$

Here χ_a is the anisotropy in the diamagnetic susceptibility, and k_{11} is the splay elastic constant. For our sample thicknesses, H_f was less than 24 G over the entire nematic temperature range. Thus the fields available to us were adequate to generate monodomain samples with the director virtually completely aligned horizontally and parallel to $\mathbf{H}$, regardless of any surface alignment.

Vertical fields for the measurement of $\lambda_\parallel$ were generated by a magnet that consisted of four horizontal coils with their vertical axes coincident with the axis of the apparatus. The coils were designed so as to provide a field that was uniform within 0.1% over a radial distance of 5 cm, spanning the entire sample, near the horizontal midplane of the magnet. Using a Hewlett Packard Model 6024A power supply, fields up to 400 G could be generated with this system. This was 17 times larger than the relevant Fréedericksz field, and produced monodomain samples with nearly homeotropic alignment. Measurements in the vertical field were made as a function of H, and could easily be extrapolated to infinite field.

C. Method of measurement and data analysis

The temperature of the Neslab refrigerated circulator was set by an analog voltage generated by a digital-to-analog (D-A) converter in the controlling computer (IBM compatible 286). This temperature determined the steady-state bath-heater power required for a given bath temperature. The bath temperature, as indicated by the bath thermistor, was sensed by a computer-interfaced multimeter (Keithley Model 196), and an appropriate power was applied to the bath heater via a D-A converter and a Hewlett Packard Model 6024A power amplifier. Once every 30 s a power increment was computed as a sum of two terms. One term was proportional to the distance of the actual temperature from the setpoint, and the other was proportional to the time derivative of the temperature. In steady state, typically between 30 and 100 W were dissipated in the bath heater. The rms temperature fluctuation of the bath usually was about 0.3 mK.

The bottom-plate temperature, as indicated by its thermistor, was also sensed by a computer-interfaced multimeter (Keithley Model 196). The thermal relaxation time of the empty cell depended primarily on the heat capacity of the bottom plate and the conductance of the sidewall. In cell 3, it was measured to be 12 min upon heating by the bottom-plate heater and 10 min upon cooling by conduction through the sidewalls and the air. Thus, for measurements of the empty-cell conductance, thermal equilibration times of about 100 min were required for a precision of order 0.1%. Typically, 2 h were allowed for the bottom plate to reach a steady-state temperature, either with zero or with a finite applied heat current. Relaxation times were shorter by a factor of about 2 when the cell was filled with 5CB, and correspondingly shorter equilibration times were used. The bottom-plate temperature was measured once a minute so that the entire thermal history of the experiment was available for analysis. The bottom-plate heater power was generated by a D-A converter and a HP Model 6024A power amplifier. The precise power used for a given point was measured by determining the voltage across the four-lead heater with a computer-interfaced Keithley Model 196 multimeter.

We calibrated the resistances of the bath and bottom-plate thermistors and of the bottom-plate heater against a Hewlett Packard Model 2804A quartz thermometer. For this purpose, an alternate top plate was made for the apparatus. The quartz thermometer was inserted through this plate, so that it was located in the water bath immediately above the sapphire sample top. The quartz-thermometer temperature scale had been adjusted to read 0.010 °C at the triple point of water. An independent comparison with a Leeds and Northrup Model 8164-B platinum thermometer calibrated against an NBS-traceable standard showed that these two temperature scales agreed within ±0.002 °C over the range from 20 to 50 °C. The precision of the calibration was about 0.001 °C.

The resistance of each of the thermistors was fit to

$$R = R_0 \exp\{[\alpha+\beta(T-T_0)+\gamma(T-T_0)^2](T-T_0)/T\} , \tag{3}$$

where T is the temperature in kelvin. Deviations from the fit over the range 12 to 52 °C were no larger than 0.001 °C. This relation for $R(T)$ was used even though one for $T(R)$ would be more convenient, since we do not know of an expression for $T(R)$ with the same number of parameters which fits the data equally well. In order to obtain T from R, Eq. (3) was inverted numerically.

The heater resistance was represented by a simple polynomial in $T-T_0$. It varied only by about 0.016%/°C.

D. Thermal conductance of the sidewall and the thermal conductivity of water

Before filling the cell, we measured the conductance $Q/\Delta T$ of the empty system. Results for cell 3 are shown in Fig. 3. At each bath temperature, the conductance was measured at two power levels, yielding temperature differences of approximately 1.3 and 2.6 °C and the pairs of points in the figure. There is no systematic dependence on the power, indicating that convection in the air in the sample space (which should not occur until much larger temperature differences are reached) was indeed negligible. The conductance of the empty system was used to obtain the wall conductance $(Q/\Delta T)_w$ by subtracting the air contribution $(Q/\Delta T)_{\rm air}=\lambda_{\rm air} A/d$, with $A/d=136.6$ cm for cell 2 and 168.3 cm for cell 3 and with [24]

$$\lambda_{\rm air}=(2.41\times10^{-4}+7.4\times10^{-7}T)\ \text{W/(cm °C)} , \tag{4}$$

with T in °C.

The measurement of the wall conductance described above is not strictly equivalent to the wall conductance of the system when filled with a fluid. For the empty cell, there is a thin layer of air (perhaps 0.001 cm) in series with the Delrin sidewalls. Probably more importantly there is a small gap near the top and bottom plate at the lateral position between the O-ring and the outside of the Delrin sidewall. These air-filled spaces become filled with fluid when the cell is filled, thus changing the conductance of the sidewalls. In the test experiments to be described below where the cell was filled with water, this was a very small effect because the conductivity of water

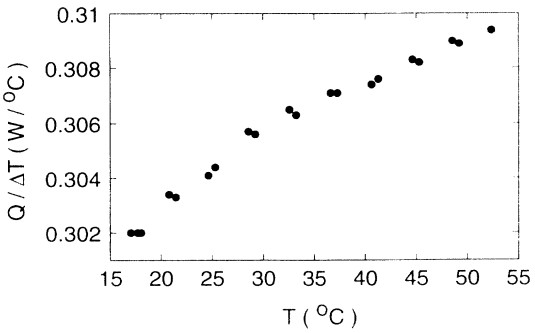

FIG. 3. Conductance of the empty cell.

is large and the conductance of the walls is relatively unimportant. However, when the cell was filled with 5 CB, the conductance of the walls was comparable to the conductance of the fluid, and even a small change had a significant effect. A rough estimate suggests that systematic errors of about 1% in $\lambda_{\parallel}$ and $\lambda_{\perp}$ and 0.4% in $\lambda_{\parallel}/\lambda_{\perp}$ may arise from this effect.

As an overall test of our procedures and the performance of the apparatus, cell 3 was filled with deionized degassed water, and the conductance was measured using temperature differences well below those corresponding to the onset of convection. The effective conductance $(Q/\Delta T)_{\text{eff}}$ of the area of the system containing the fluid was obtained by subtracting the wall conductance given above. If it were not for the series resistance of the sapphire and the thermal boundary layer above the sapphire, this would be the conductance of the water. We corrected for the resistance of the sapphire, using the sapphire conductivity λ_s in the form

$$\lambda_s = (0.45 - 0.0025T)\ \text{W/(cm °C)}\ , \tag{5}$$

which is a good approximation over the range $10\,°\text{C} \le T \le 50\,°\text{C}$. Neglecting the resistance of the boundary layer in the bath above the sapphire, and recognizing that for cell 3 the thickness of the sapphire is essentially the same as that of the water layer, the conductivity of the water is then given by

$$\lambda_{\text{water}} = 1/[(1/\lambda_{\text{tot}}) - (1/\lambda_s)]\ , \tag{6}$$

with $\lambda_{\text{tot}} = (Q/\Delta T)_{\text{eff}} d/A$. The correction for the sapphire resistance is approximately 1.6%. We estimate that the correction for the boundary resistance is smaller by a factor of 4, and we neglect it because it is known only within a factor of 2 or so. The results for λ_{water} are shown in Fig. 4 as solid circles. Values tabulated in the literature [25] are given by the solid line. The difference between the data and the accepted values is of the same order as the neglected boundary resistance. It is also only a factor of 2 larger than the uncertainty in our cell thickness. Thus we conclude that our method yields reliable values of the thermal conductivity of the fluid in the cell.

Finally we remark that the conductivity of 5CB is smaller than that of water by about a factor of 4. Thus the correction for the resistance of the sapphire and the boundary layer will be relatively smaller by this factor (about 0.5% rather than 2% total). In evaluating the conductivity of 5CB, the correction for the finite sapphire conductivity will be applied; the correction for the boundary layer (about 0.1%) will be neglected.

After these preliminary tests, cell 3 was disassembled, dried, reassembled, and the conductance of the empty system was remeasured. The reproducibility of the conductance after reassembly was about 1%. The cell was then filled with 5CB [26]. We measured the clearing point on our temperature scale and found it to be 35.17 °C.

III. RESULTS AND DISCUSSION

Figure 5 shows the results for $\lambda_{\perp}$ for $T < T_{NI}$, as well as of the isotropic conductivity λ for $T > T_{NI}$. These results were obtained in the horizontal field of the Varian magnet, with $H \gtrsim 1000$ G. The squares were measured with cell 2, whereas the circles correspond to cell 3. The agreement between the data obtained with the two cells is gratifying, since each measurement is dependent upon a correct determination of the conductivity of the empty cell. We regard the results for cell 3 as more accurate and precise than those for cell 2, and thus give them in numerical form in Table I.

Since we wanted to measure both $\lambda_{\parallel}$ and $\lambda_{\perp}$, we made no attempt during the construction of the conductivity cell to produce a particular surface alignment of the director. Instead, we used a large enough magnetic field in the appropriate direction to force essentially complete alignment parallel to the field throughout the cell. Thus, it is important to ascertain that the data were obtained in a sufficiently high field. The solid circles in Fig. 5 were measured in cell 3 with an applied horizontal field of 1420 G. For the open circles, 750 G was used. The good agreement between the two data sets shows that both correspond essentially to the high-field limit where the sample is a single domain with the director perpendicular to the heat current.

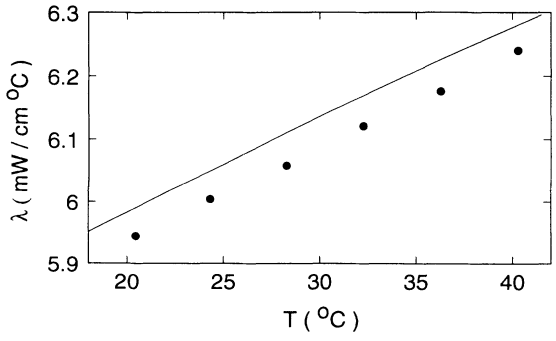

FIG. 4. Thermal conductivity of water. The solid line is the accepted result.

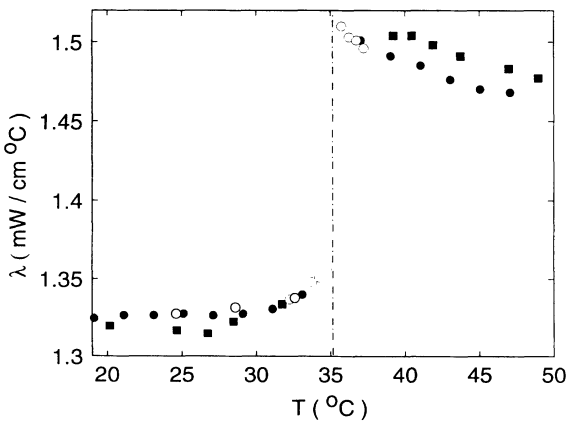

FIG. 5. Thermal conductivity of 5CB in a horizontal field. The squares are for cell 2, and the circles for cell 3. The solid symbols were measured in a field of about 1420 G, whereas the open circles correspond to 750 G.

In order to measure $\lambda_{\parallel}$, the apparatus was moved out of the Varian magnet and surrounded by the coils. Only cell 3 was used in this configuration. In this system, the largest field available was 400 G, or about $17H_f$. Therefore, we measured the conductivity as a function of H at a fixed temperature. Starting with a multidomain sample containing many defects, we found λ to be field dependent. This is illustrated in Fig. 6, which shows the temperature difference across the sample in the presence of a heat current of 1 W. The field was stepped at 2-h intervals from zero in increments of 25 G. For small fields, there were very slow relaxation effects during which the conductivity increased gradually. We attribute these relaxations to the slow removal of defects. Above about 200 G, the relaxation times became short and of the same size as thermal relaxation times. This can be seen in the lower portion of Fig. 6, which is an expanded view of the data shown in the top part of the figure. In this field range, we believe that we have a monodomain sample with a field-dependent conductivity.

TABLE I. Experimental results for the conductivities. The data are given in the order in which they were measured.

T (°C)	λ (mW/cm °C)
Results obtained in a horizontal field	
21.13	1.351
23.13	1.350
25.13	1.350
27.13	1.348
29.13	1.348
31.12	1.349
33.12	1.357
37.06	1.507
39.06	1.497
41.06	1.491
43.06	1.482
45.06	1.476
20.63	1.350
24.63	1.350
32.62	1.355
32.27	1.354
32.78	1.355
33.28	1.357
33.78	1.364
34.27	1.366
34.78	1.370
36.26	1.509
36.76	1.507
37.26	1.502
Results obtained in a vertical field	
19.09	2.359
21.09	2.331
23.10	2.296
25.10	2.260
27.11	2.218
29.12	2.171
31.14	2.114
33.16	2.037
37.33	1.507
31.27	2.116
31.77	2.095
32.27	2.077
32.77	2.055
33.27	2.030
33.78	2.009
34.78	1.941
35.81	1.512
36.31	1.507
36.81	1.505

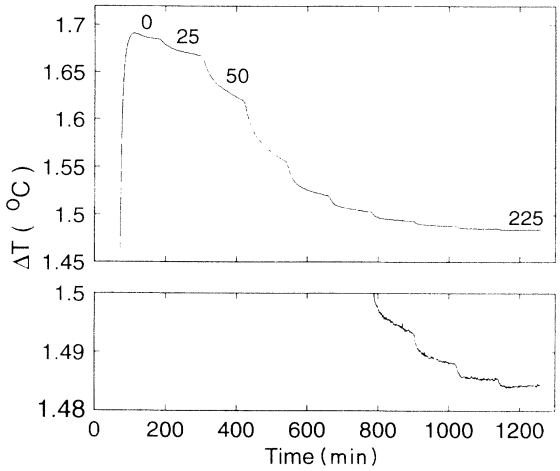

FIG. 6. The temperature difference across cell 3 with an applied heat current of 1 W. The sample initially had many domains and defects. Successively higher fields, in steps of 25 G, were applied at 2-h intervals (a few field values are indicated in the figure). For fields up to 200 G, long relaxation times suggest the annealing of defects. For larger fields, a steady state was reached on a time scale determined by the thermal diffusion time. The lower portion of the figure shows the data on an expanded vertical scale.

Although we do not know the surface alignment in our case, it is instructive to compare our steady-state measurements with a theoretical result by Deuling [27] for the case of parallel surface alignment and a vertical field. His Eq. (42) for the high-field limit can be written as

$$\lambda_{\text{eff}}=\lambda_{\parallel}\times[1+S_1/H+O(1/H^2)+\cdots], \tag{7}$$

with

$$S_1=[(\lambda_{\parallel}/\lambda_{\perp})^{1/2}-1]H_f . \tag{8}$$

Here H_f is the Fréedericksz field given by Eq. (2), and λ_{eff} is the effective, i.e., measured, conductivity. Figure 7 shows our steady-state results for λ_{eff} at a mean temperature of 26.11 °C, plotted as a function of $1/H$. The solid symbols correspond to increasing, and the open ones to decreasing fields. The squares and circles are for two different experimental runs on different days. A least-squares fit to

$$\lambda_{\text{eff}}=\lambda_{\parallel}\times(1+S_1/H+S_2/H^2) \tag{9}$$

yielded the solid line. Parameters obtained from such fits to data at three temperatures are collected in Table II. Also given there are the corresponding theoretical results

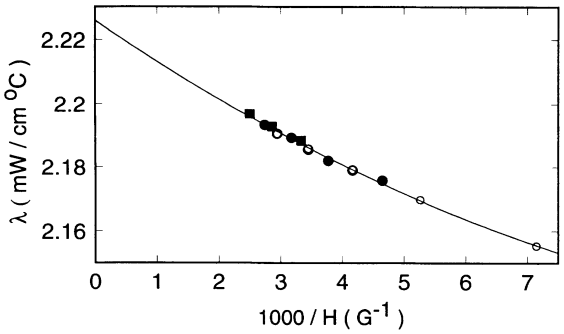

FIG. 7. Steady-state values of λ at 26.11 °C in the presence of a vertical field H as a function of $1/H$. Squares and circles are two separate runs. Solid (open) circles correspond to increasing (decreasing) field values.

S_1^{th}, and the values [28–30] of H_f and $\lambda_\parallel/\lambda_\perp$ which were used to calculate S_1^{th}. As can be seen, the experimental value for S_1 is somewhat larger than the theoretical one, presumably because of deviations from a parallel orientation of the director at the surfaces. To complement these results, we also made a few measurements of λ_{eff} in a horizontal field as a function of H. They too could be fit to Eq. (9), and at 24.4 °C they gave $S_1 = 1.86$ G, i.e., a value of somewhat smaller magnitude and of the opposite sign. The fact that λ_{eff} depends upon H with H both parallel and perpendicular to the heat current indicates that the director alignment at the top and/or bottom surfaces is neither perfectly parallel nor perfectly perpendicular to the surfaces. This is not surprising since we had made no attempt to achieve one alignment or the other. The reproducibility of $\lambda_{eff}(H)$ with increasing and decreasing H indicates that the field dependence is not due to the further elimination of defects, and is consistent with a monodomain sample.

Most of the measurements in the vertical field were made at 400 G. We see from Fig. 7 that they are within about 1% of $\lambda_\parallel$. They were extrapolated to the high-field limit using Eq. (9).

Results for $\lambda_\parallel$ are shown in Fig. 8, together with the data for $\lambda_\perp$ and measurements in the isotropic phase in both horizontal and vertical fields. As is expected, the data above T_{NI} are field independent. Below T_{NI}, $\lambda_\parallel$ is considerably larger than $\lambda_\perp$. The data for $\lambda_\parallel$ are also tabulated in Table I. Since the behavior of the conductivities near T_{NI} is of particular interest, we show the data near the transition on an expanded scale in Fig. 9. The results clearly show that the conductivities are discontinuous at T_{NI}, as would be expected for a first-order

TABLE II. Parameters for Eq. (9). See text for details.

Parameter \ T (°C)	19.09	26.11	33.0
$\lambda_\parallel$ (mW/cm K)	2.337	2.226	2.022
S_1 (G)	−5.55	−5.88	−3.70
S_2 (G²)	120	200	53
$\lambda_\parallel/\lambda_\perp$	1.77	1.68	1.51
H_f (G)	23.5	21.9	19.0
S_1^{th} (G)	−7.73	−6.49	−4.36
S_1/S_1^{th}	0.72	0.91	0.85

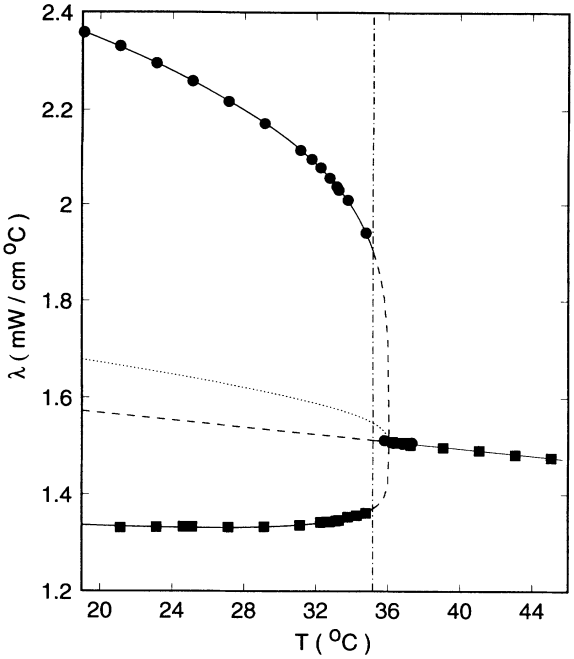

FIG. 8. Measured conductivities $\lambda_\perp$ (squares) and $\lambda_\parallel$ (circles) of 5CB. For $T > T_{NI} = 35.17$ °C, both sets of measurements give the conductivity of the isotropic phase. The solid lines are the fit of Eqs. (10) and (11) to the data. The dashed lines are extrapolations of that fit into the unstable regions. The vertical dash-dotted line is the transition temperature T_{NI}. The dotted line is the result for $(\lambda_\parallel + 2\lambda_\perp)/3$.

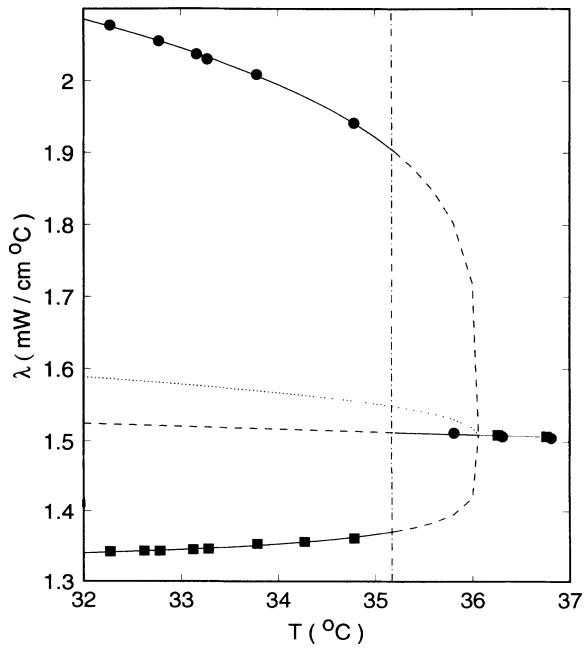

FIG. 9. An expanded view of Fig. 8 in the vicinity of T_{NI}.

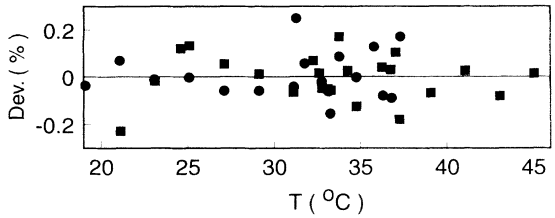

FIG. 10. Relative deviations $(\lambda-\lambda_{fit})/\lambda_{fit}$ of the data from the fit Eqs. (10) and (11). The symbols are as in Figs. 8 and 9.

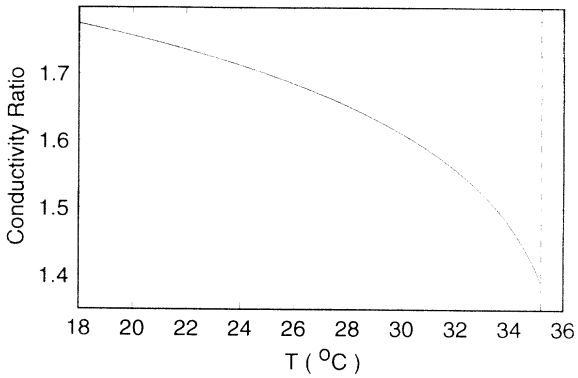

FIG. 11. The conductivity ratio $\lambda_{\parallel}/\lambda_{\perp}$ as a function of the temperature.

transition. They do suggest, however, a power-law singularity at a temperature $T_c > T_{NI}$ which is not reached because the first-order transition intervenes.

It is often useful to have a closed-form expression which fits the thermal-conductivity data well. Thus we fit the data to the empirical function

$$\lambda=\lambda_0+\lambda_1\times(T-T_{NI})+\lambda_s \ , \tag{10a}$$

where λ_s is a singular contribution. The clearing point T_{NI} had been determined independently by visual observation, and had been found to be 35.17 °C on our temperature scale. For $T > T_{NI}$, there was no evidence in the data for a singular part, and λ_s was set equal to zero. Below T_{NI}, we used

$$\lambda_{s,\parallel}=\lambda_{1,\parallel}(T_c-T)^{\alpha_\parallel} \tag{10b}$$

for $\lambda_{\parallel}$ and

$$\lambda_{s,\perp}=\lambda_{1,\perp}(T_c-T)^{\alpha_\perp} \tag{10c}$$

for $\lambda_{\perp}$. A fit to all the data gave the parameters

$$\lambda_0=1.512 \ , \tag{11a}$$

$$\lambda_1=-0.003\,70 \ , \tag{11b}$$

$$\lambda_{1,\parallel}=0.4026 \ , \tag{11c}$$

$$\lambda_{1,\perp}=-0.1448 \ , \tag{11d}$$

$$T_c=36.06\pm0.06 \ , \tag{11e}$$

$$\alpha_\parallel=0.237\pm0.004 \ , \tag{11f}$$

$$\alpha_\perp=0.172\pm0.005 \ . \tag{11g}$$

Relative deviations from the fit are shown in Fig. 10. They are generally less than 0.2%, with a standard deviation of 0.10%. Note that we do not attach any physical significance to the parameters of the fit; we obtained them so as to have convenient expressions for the conductivities. Nonetheless, we remark that forcing $\alpha_\parallel=\alpha_\perp$ caused systematic deviations of the data from the fit and increased the standard deviation to 0.21%. In Figs. 8 and 9, the fits are shown as continuous lines. The solid (dashed) lines correspond to the physical extrapolated regions of the three branches of the conductivity.

The dotted line in Figs. 8 and 9 represents the quantity $(\lambda_\parallel+2\lambda_\perp)/3$, which might be expected to coincide with an extrapolation of λ from above T_{NI}, i.e., with the dashed line below T_{NI}. As can be seen, the agreement is not particularly good.

The results for the two conductivities below T_{NI} give the anisotropy $\lambda_\parallel/\lambda_\perp$ which is needed in the theory of Rayleigh-Bénard convection of a nematic liquid crystal. We show $\lambda_\parallel/\lambda_\perp$ based on the fit to our data as a function of T in Fig. 11.

Finally, we compare our results with previous measurements. Using stimulated Rayleigh scattering [10,11], the thermal diffusivities $\kappa_{\parallel,\perp}=\lambda_{\parallel,\perp}/\rho C_p$ were measured by Urbach [10] to be $\kappa_\parallel=(12.5\pm0.5)\times10^{-4}$ and $\kappa_\perp=(7.9\pm0.4)\times10^{-4}$ cm^2/s at 25 °C. Using $C_p=1.92$ J/g K for the heat-capacity per unit mass [31,32] and $\rho=1.022$ g/cm^3 for the density [33], these results give $\lambda_\parallel=2.40\pm0.1$ and $\lambda_\perp=1.52\pm0.08$ mW/cm K. These values are somewhat higher than our results $\lambda_\parallel=2.219\pm0.044$ and $\lambda_\perp=1.326\pm0.027$ mW/cm K.

ACKNOWLEDGMENTS

We are grateful to S. W. Morris for many helpful discussions about nematic liquid crystals, and to G. Ramian for calculations used in the design of the vertical-field magnet and the pole pieces of the Varian magnet. One of us (L.I.B.) thanks the Norwegian Research Council for Sciences and the Humanities for support. One of us (S.S.) acknowledges support from the Ministry of Education of Japan. This work was supported by the National Science Foundation through Grant No. DMR91-17428.

[1] For an authoritative discussion of the nematic state, see P. G. de Gennes, *The Physics of Liquid Crystals* (Clarendon, Oxford, 1973).
[2] E. Dubois-Violette, E. Guyon, and P. Pieranski, Mol. Cryst. Liq. Cryst. **26**, 193 (1973).
[3] P. Pieranski, E. Dubois-Violette, and E. Guyon, Phys. Rev. Lett. **30**, 736 (1973).
[4] E. Guyon, P. Pieranski, and J. Salan, J. Fluid. Mech. **93**, 65 (1979).
[5] J. Salan and E. Guyon, J. Fluid. Mech. **126**, 13 (1983).
[6] K. Otnes and T. Riste, Physica **120B**, 376 (1983).
[7] P. J. Barratt, Liq. Cryst. **4**, 223 (1989).
[8] Q. Feng, W. Pesch, and L. Kramer, Phys. Rev. A **45**, 7242 (1992).
[9] L. I. Berge, G. Ahlers, and D. S. Cannell, Phys. Rev. E **48**, 3236 (1993).
[10] W. Urbach, Ph.D. thesis, University of Paris–South, Orsay, France, 1981 (unpublished).
[11] W. Urbach, H. Hervet, and F. Rondelez, Mol. Cryst. Liq. Cryst. **46**, 209 (1978).
[12] P. Pieranski, F. Brochard, and E. Guyon, J. Phys. (Paris) **33**, 681 (1972).
[13] R. Villanove, E. Guyon, C. Mitescu, and P. Pieranski, J. Phys. (Paris) **35**, 153 (1974).
[14] J. Thoen, C. Glorieux, E. Schoubs, and W. Lauriks, Mol. Cryst. Liq. Cryst. **191**, 29 (1990).
[15] S. Chandrasekhar, *Hydrodynamic and Hydromagnetic Stability* (Oxford University Press, London, 1961).
[16] C. W. Meyer, G. Ahlers, and D. S. Cannell, Phys. Rev. A **44**, 2514 (1991).
[17] Most of the dimensions are approximately to scale. However, the main body of the apparatus was somewhat longer than shown. In addition, the base was thicker and more intricate than shown since it accomodated the electrical feedthroughs.
[18] The use of PVC limits the temperature range to 50 °C or less since this material becomes soft at higher temperature. The use of CPVC (postchlorinated PVC) or Delrin, although more costly, would allow higher operating temperatures.
[19] We used Fenwal Model GA51M2 thermistors, which have a resistance of $\approx 100\ k\Omega$ at room temperature.
[20] H. R. Haller, C. Destor, and D. S. Cannell, Rev. Sci. Instrum. **54**, 973 (1983).
[21] General Magnaplate Corp., 1331 Route 1, Linden, NJ 07036.
[22] We used Thermofoil heaters manufactured by Minco Products Inc., 7300 Commerce Lane, Minneapolis, MN 55432.
[23] We used Teflon tubing and chemically inert flanged tube assemblies from Rainin Instrument Co., Mack Road, Woburn, MA 01801.
[24] See, for instance, *Handbook of Chemistry and Physics,* 57th ed. (CRC, Cleveland, OH, 1976), p. E-2.
[25] See, for instance, *Handbook of Chemistry and Physics,* 57th ed. (CRC, Cleveland, OH, 1976), p. E-11.
[26] We obtained the 5CB from EM Industries, 5 Skyline Drive, Hawthorne, NY 10532.
[27] H. J. Deuling, *Liquid Crystals, Solid State Phys. Supplement,* edited by L. Liebert (Academic, New York, 1978), Vol. 14, p. 77.
[28] In order to estimate H_f from Eq. (2), we used the data of Sherrell and Crellin [29] for χ_a and the values of k_{11} from Bradshaw *et al.* [30].
[29] P. L. Sherrell and D. A. Crellin, J. Phys. (Paris) Colloq. **40**, C3-211 (1979).
[30] M. J. Bradshaw, E. P. Raynes, J. D. Bunning, and T. E. Faber, J. Phys. (Paris) **46**, 1513 (1985).
[31] J. Thoen, in *Phase Transitions in Liquid Crystals,* edited by S. Martellucci (Plenum, New York, 1992).
[32] G. S. Iannacchione and D. Finotello, Phys. Rev. Lett. **69**, 2094 (1992).
[33] D. A. Dunmur and W. H. Miller, J. Phys. (Paris) Colloq. **40**, C3-141 (1979).